Electronic Supplementary Information (ESI)

An Ethynyl-Modified Interpenetrated Metal-Organic Framework for Highly Efficient Selective Gas Adsorption

Xueyue Yu,[a] Ziyang Huang,[b] Rajamani Krishna,[C] Xiaolong Luo*[a, b] and Yunling Liu*[a]

[a] State Key Laboratory of Inorganic Synthesis & Preparative Chemistry, Jilin University, Changchun 130012, P. R. China

E-mail: yunling@jlu.edu.cn; Fax: +86 431 85168624

[b] School of Chemistry and Life Science, Advanced Institute of Materials Science, Changchun University of Technology, Changchun, 130012, P. R. China

[C] Van 't Hoff Institute for Molecular Sciences, University of Amsterdam, Science Park 904, 1098 XH Amsterdam, The Netherlands.

E-mail: r.krishna@contact.uva.nl

Calculation procedures of selectivity from IAST

The ideal adsorption solution theory (IAST) was used to predict the binary mixture adsorption from the experimental pure-gas isotherms. The single-component isotherms were fitted using a dual-site Langmuir-Freundlich (DSLF) equation:

$$q = q_{m1} \cdot \frac{b_1 \cdot p^{1/n_1}}{1 + b_1 \cdot p^{1/n_1}} + q_{m2} \cdot \frac{b_2 \cdot p^{1/n_2}}{1 + b_2 \cdot p^{1/n_2}}$$

Here, p is the pressure of the bulk gas at equilibrium with the adsorbed phase (kPa), q is the adsorbed amount per mass of adsorbent (mmol/g), q_{m1} and q_{m2} are the saturation capacities of sites 1 and 2 (mmol/g), b_1 and b_2 are the affinity coefficients of sites 1 and 2 (1/kPa), and n_1 and n_2 represent the deviations from an ideal homogeneous surface.

To investigate the separation of binary mixtures, the adsorption selectivity is defined as follows equation:

$$S = \frac{q_1/q_2}{p_1/p_2}$$

Where q_i and p_i (i=1, 2) are the mole fractions of component 1 and 2 in the adsorbed and bulk phases, respectively. The IAST calculations were carried out for binary mixture containing equimolar gas.

Calculations of the Isosteric Heats of Gas Adsorption (Q_{st}):

A virial-type[30] expression comprising the temperature-independent parameters a_i and b_j was employed to calculate the enthalpies of adsorption for CO_2, CH_4, C_2H_6, C_3H_8, C_2H_4 and C_2H_2 (at 273and 298 K) on compounds. In each case, the data were fitted using the equation:

$$ln^P = ln^N + {}^1/_T \sum_{i-0}^{m} a_i N^i + \sum_{j-0}^{n} b_j N^j$$

Here, P is the pressure expressed in Torr, N is the amount adsorbed in mmol g^{-1}, T is the temperature in K, a_i and b_j are virial coefficients, m, n represent the number of coefficients required to adequately describe the isotherms (m and n were gradually increased until the contribution of extra added a and b coefficients was deemed to be statistically insignificant towards the overall fit, and the average value of the squared deviations from the experimental values was minimized). The values of the virial coefficients a_0 through a_m were then used to calculate the isosteric heat of adsorption using the following expression.

$$Q_{st} = -R \sum_{i-0}^{m} a_i N^i$$

Q_{st} is the coverage-dependent isosteric heat of adsorption and R is the universal gas constant. The heat of gas sorption for compound **1** in this manuscript are determined by using the sorption data measured in the pressure range from 0-1 bar (273 and 298 K for gases), which is fitted by the virial-equation very well.

Transient breakthrough simulations

Transient breakthrough simulations were carried out using the methodology described in earlier publications.[1-5] In these simulations, intra-crystalline diffusion influences are ignored.

The simulations were performed in a fixed bed with the following parameters: adsorber length, L = 0.3 m; cross-sectional area, A = 1 m^2; interstitial gas velocity in the bed, v = 0.1 m s^{-1}; voidage of the packed bed, ε = 0.4; the superficial gas velocity at the inlet to the bed, u_0 = 0.04 m s^{-1}. The volumetric flow rate of the gas mixture at the inlet Q_0 = 40 L s^{-1}. The volume of MOF used in the simulations is $V_{ads} = LA(1-\varepsilon)$ = 0.18 m^3 = 180 L. The total volume of the bed is $V_{bed} = LA$. It is important to note that the volume of adsorbent, V_{ads}, includes the pore volume of the adsorbent material. If ρ is the

framework density, the mass of the adsorbent in the bed is $m_{ads} = (1-\varepsilon)\times(L\ \text{m})\times(A\ \text{m}^2)\times(\rho\ \text{kg m}^{-3})$ kg.

The mixture adsorption equilibrium were determined using the Ideal Adsorbed Solution Theory (IAST) of Myers and Prausnitz;[6] the unary isotherm data fits.

The breakthrough data are presented in terms of the dimensionless concentrations at the exit of the fixed bed, c_i/c_{i0}, as function of the modified time parameter

$$\frac{(Q_0 = \text{flow rate L s}^{-1})\times(\text{time in s})}{(\text{kg MOF packed in tube})} = \frac{Q_0 t}{m_{ads}} = \text{L kg}^{-1}.$$

Notation

L length of packed bed adsorber, m

m_{ads} mass of adsorbent packed in fixed bed, kg

Q_0 volumetric flow rate of gas mixture entering fixed bed, $m^3\ s^{-1}$

u superficial gas velocity in packed bed, $m\ s^{-1}$

v interstitial gas velocity in packed bed, $m\ s^{-1}$

Greek letters

ε voidage of packed bed, dimensionless

ρ framework density, $kg\ m^{-3}$

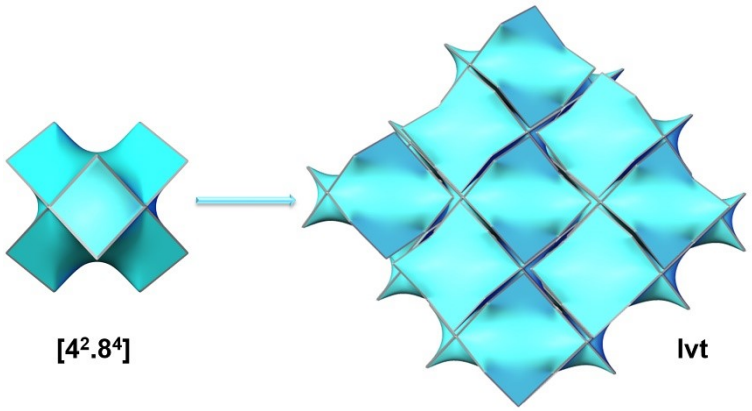

Figure S1. Topological features of compound **1** displayed by tiles and face symbols for blue tile is [$4^2.8^4$].

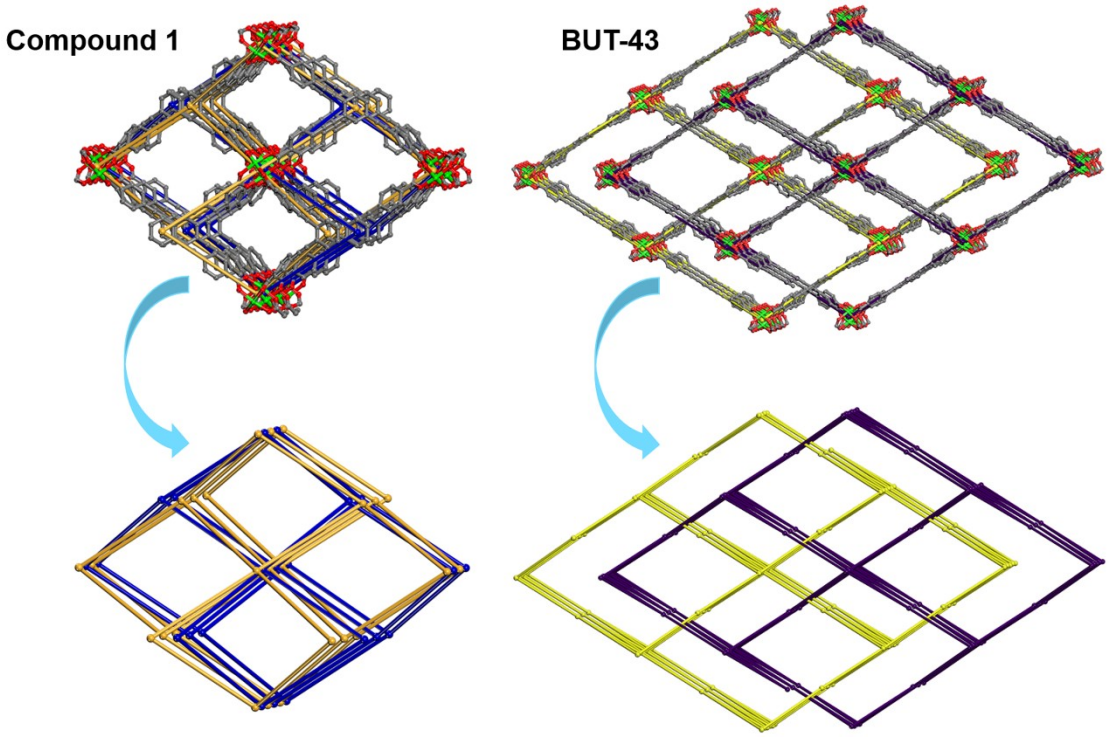

Figure S2. The difference between compound **1** and BUT-43 in the degree of interpenetration.

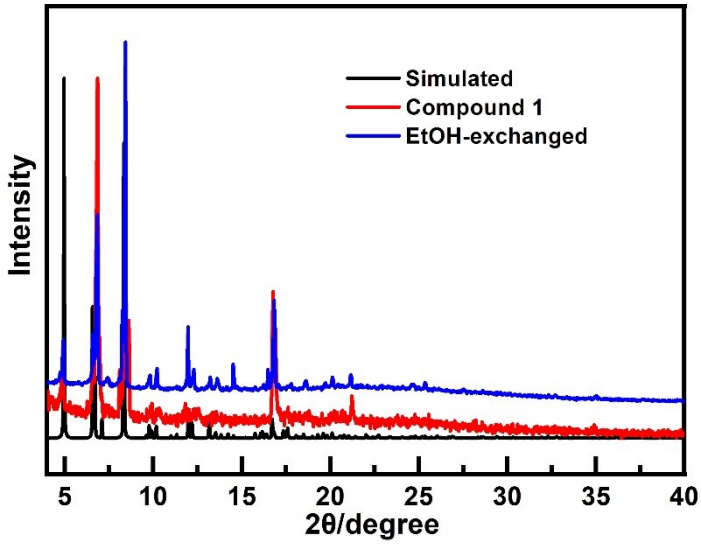

Figure S3. The PXRD patterns of simulated, as-synthesized and EtOH-exchanged.

Figure S4. Single crystal optical images of compound **1**.

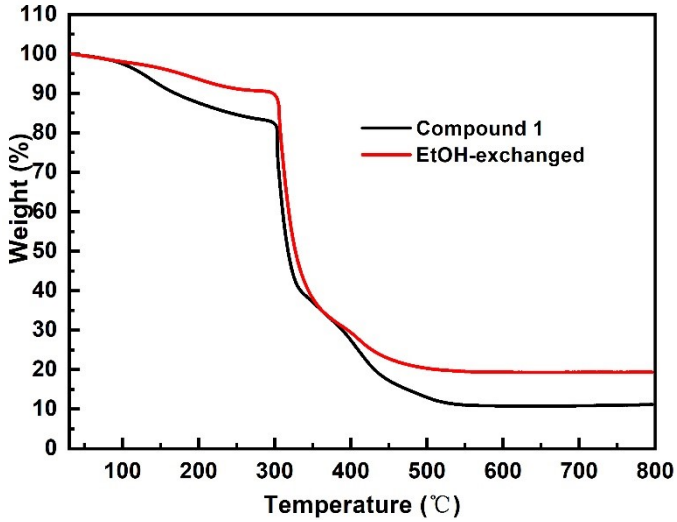

Figure S5. Thermogravimetric analysis curves of as-synthesized and after ethanol exchanged samples for compound **1**.

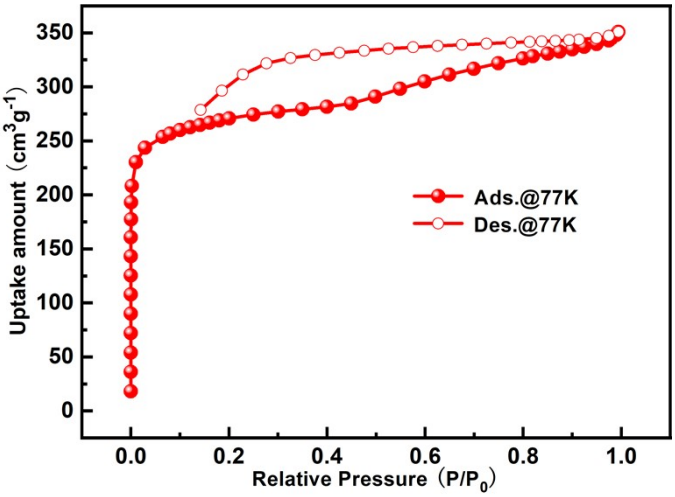

Figure S6. N_2 isotherms for compound **1** at 77 K under 1 atm.

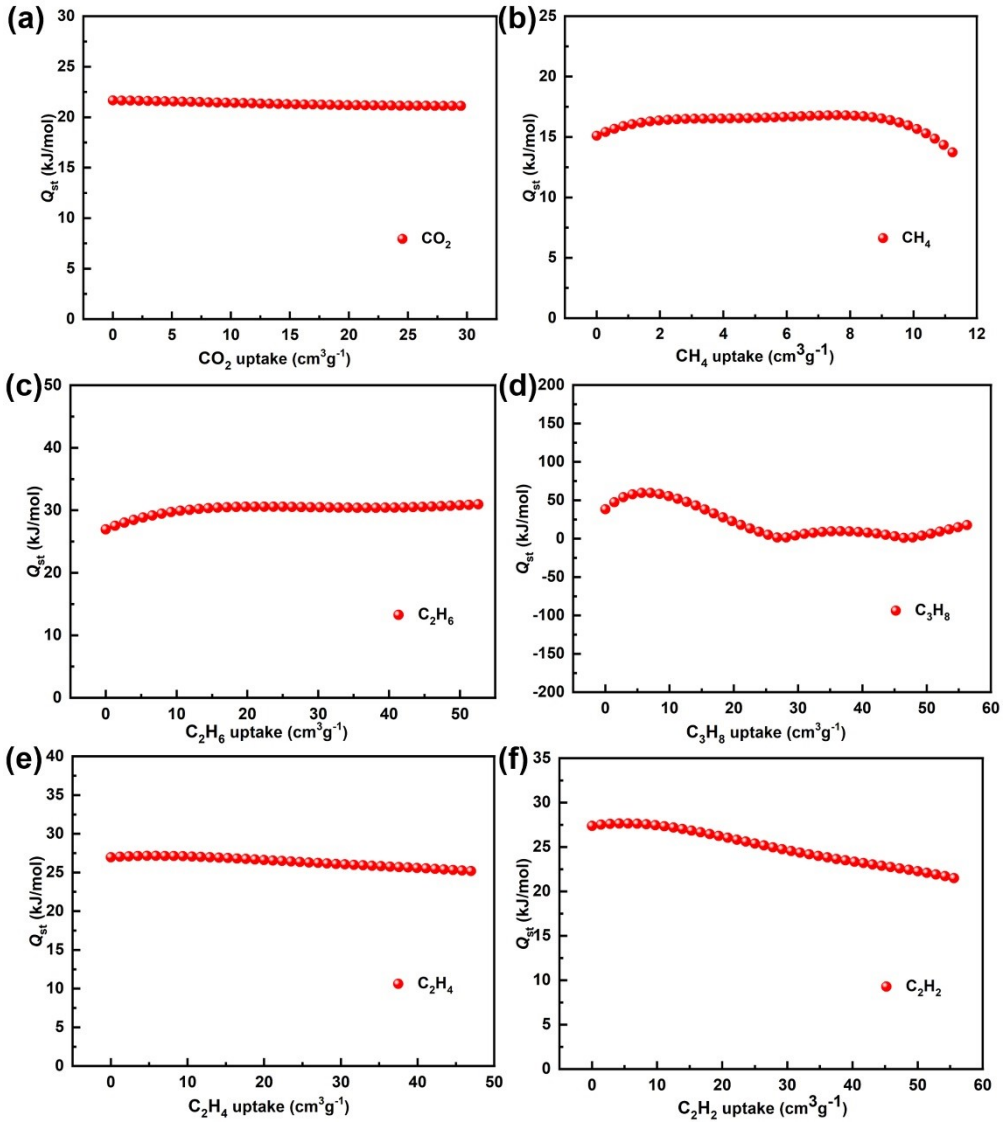

Figure S7. Q_{st} of (a) CO_2; (b) CH_4; (c) C_2H_6; (d) C_3H_8; (e) C_2H_4; (f) C_2H_2 for compound **1**.

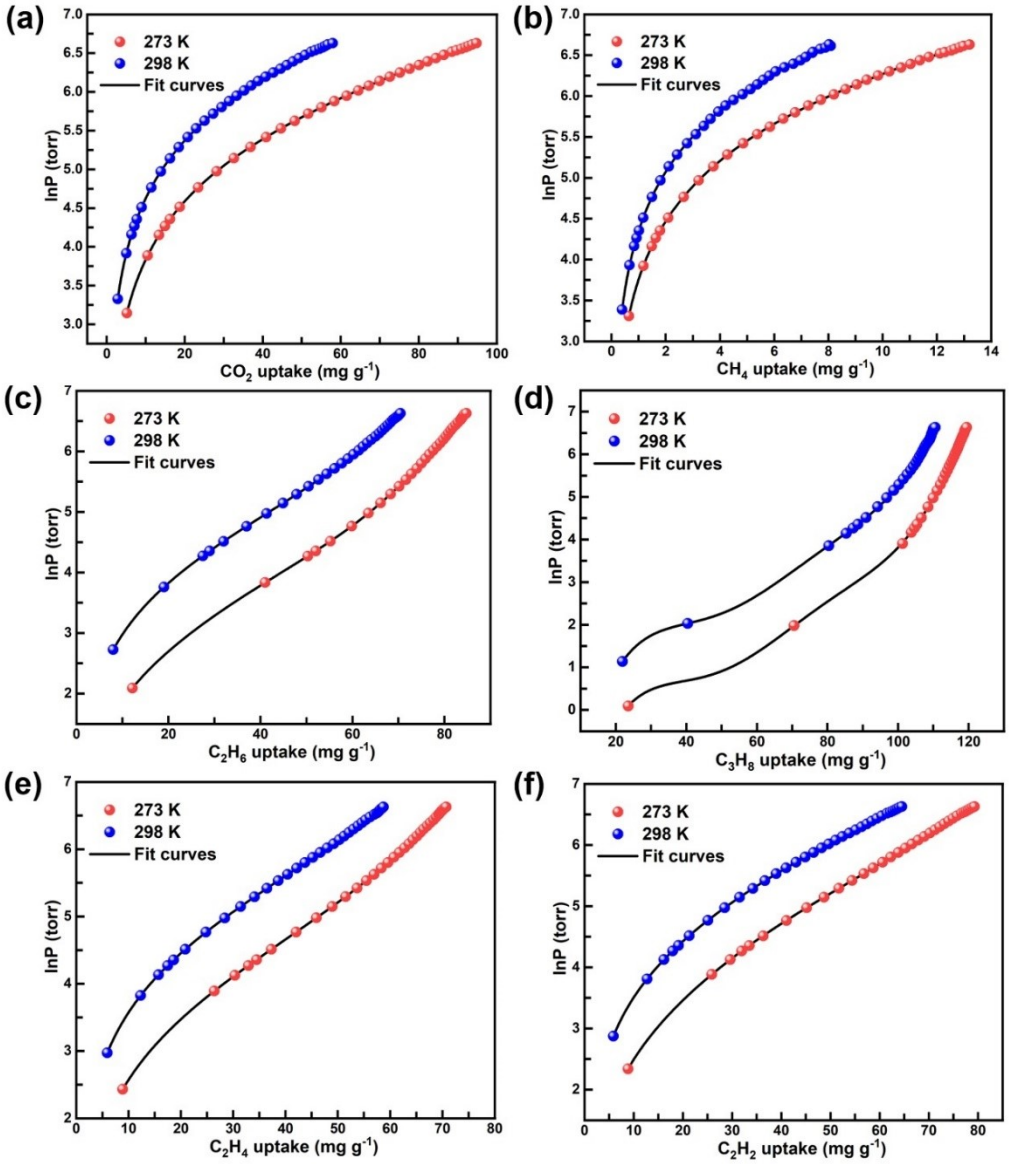

Figure S8. Nonlinear curves fitting of compound **1** for CO_2 (a), CH_4 (b), C_2H_6 (c), C_3H_8 (d), C_2H_4 (e) and C_2H_2 (f) at 273 K and 298 K.

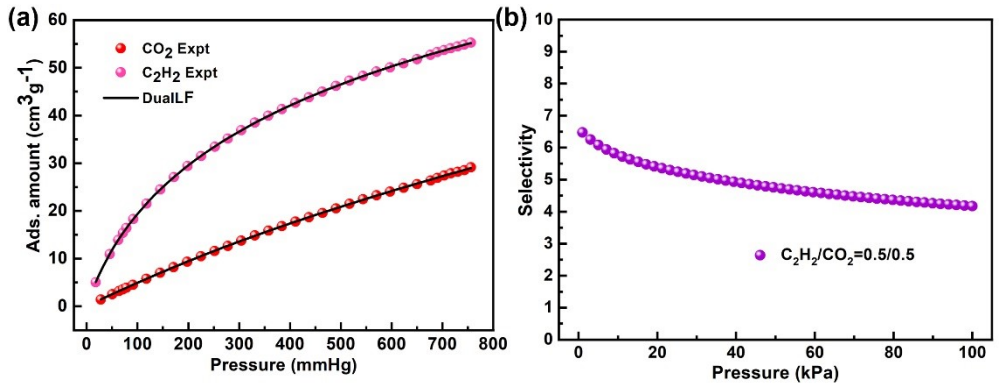

Figure S9. (a) C_2H_2 and CO_2 adsorption isotherms at 298 K along with the DSLF fits; (b) C_2H_2/CO_2 selectivity of compound **1** at 298 K by the IAST method.

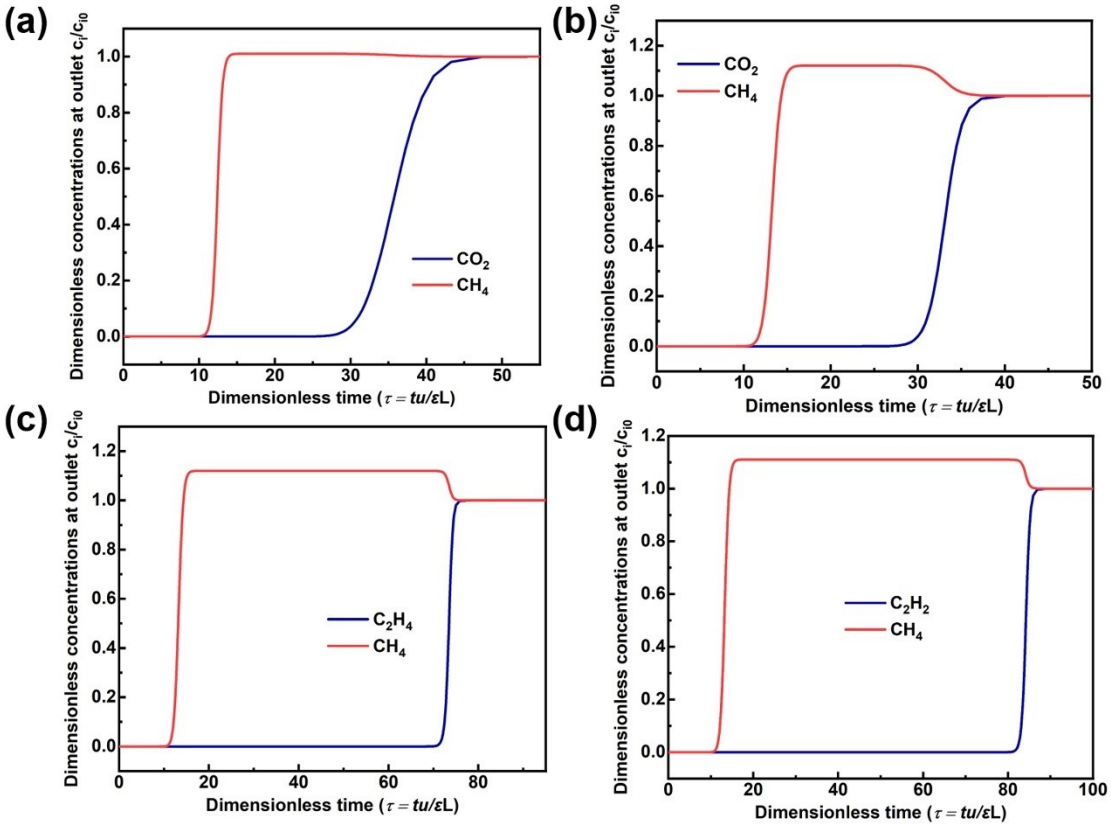

Figure S10. Transient breakthrough simulations for separation of 5/95 and 50/50 (a and b) CO_2/CH_4, 50/50 and 50/50 C_2H_4/CH_4 and C_2H_2/CH_4 (c and d) mixtures containing. The total inlet pressure is 100 kPa. The *y*-axis is the dimensionless concentrations at the exit, normalized with respect to the inlet concentrations.

Table S1. Crystallographic data and structure refinement for compound **1**.

compound	**Compound 1**
Formula	$C_{23}H_{14}CuO_5N$
Formula weight	447.90
Temperature (K)	273(2)
Wavelength (Å)	0.71073
Crystal system	Orthorhombic
Space group	*Cmca*
a (Å)	26.4044(8)
b (Å)	35.6894(11)
c (Å)	17.4068(5)
α (°)	90
β (°)	90
γ (°)	90
Volume (Å^3)	16403.4(9)
Z	16
F(000)	3648
θ range (deg)	2.21 to 23.94
reflns collected/unique	51994 / 7469
R_{int}	0.0563
data/restraints/params	3092 / 73 / 299
Goodness-of-fit on F^2	1.011
R_1, wR_2 [$I>2\sigma(I)$]	0.0489, 0.1452
R_1, wR_2 (all data)	0.0837, 0.1758

Table S2. Selected bond lengths (Å) and angles (°) for compound **1**.

Cu(1)-O(2)	1.957(2)	O(1)-Cu(1)-O(5)	93.10(10)
Cu(1)-O(4)	1.963(2)	O(3)-Cu(1)-O(5)	92.90(10)
Cu(1)-O(1)	1.960(2)	O(2)-Cu(1)-Cu(1)#1	83.76(8)
Cu(1)-O(3)	1.970(2)	O(4)-Cu(1)-Cu(1)#1	86.83(7)
Cu(1)-O(5)	2.127(3)	O(1)-Cu(1)-Cu(1)#1	84.89(8)
O(2)-Cu(1)-O(4)	89.29(10)	O(3)-Cu(1)-Cu(1)#1	81.63(7)
O(2)-Cu(1)-O(1)	168.64(11)	O(5)-Cu(1)-Cu(1)#1	174.18(7)
O(4)-Cu(1)-O(1)	89.57(9)	C(21)-O(1)-Cu(1)	121.7(2)
O(2)-Cu(1)-O(3)	89.55(10)	C(21)#1-O(2)-Cu(1)	123.1(2)
O(4)-Cu(1)-O(3)	168.46(10)	C(1)#1-O(3)-Cu(1)	125.8(2)
O(1)-Cu(1)-O(3)	89.31(10)	C(1)-O(4)-Cu(1)	120.4(2)
O(2)-Cu(1)-O(5)	98.25(10)	C(22A)-O(5)-Cu(1)	121.7(6)
O(4)-Cu(1)-O(5)	98.63(10)	C(22B)-O(5)-Cu(1)	120.8(4)

Symmetry transformations used to generate equivalent atoms: #1 -x+y,-x+1,z #2 -y+1,x-y+1,z #3 y,-x+y,-z+1 #4 y,-x+y,z-1/2 #5 x,y,-z+1/2 #6 x-y,x,-z+1 #7 x,y,-z+3/2

Table S3. Comparison of the crystal data for compound **1** and BUT-43

Compound	Compound **1**	BUT-43
Formula	$C_{23}H_{14}CuO_5N$	$C_{42}H_{22}Cu_2O_{10}$
Crystal system	Orthorhombic	Monoclinic
Space group	*Cmca*	*C*2/*c*
a (Å)	26.4044(8)	42.7195(15)
b (Å)	35.6894(11)	23.6272(18)
c (Å)	17.4068(5)	21.5936(9)
α (°)	90	90
β (°)	90	120.317
γ (°)	90	30
V (Å³)	16403.4(9)	18814.8(19)

Table S4. C_3H_8/CH_4 selectivity performance comparison of some previous reported MOFs.

Compound	**Selectivity (0.5:0.5)**	**Ref.**
MIL-142A	1300	7
LSHU01’	912.6	8
ZUL-C2	632	9
BSF-1	353	10
JLU-MOF66	308.4	11
Cu-IPA	296	12
JLU-MOF67	287.1	11
JLU-MOF51	220	13
Compound **1**	204.7	This work
CTGU-15	170.7	14
FJI-H21	145.2	15
NUM-18a	109	16
ANPC-1-800	110.4	17
Zr-OBBA	105.6	18
Zr-SDBA	97.5	18
FIR-7a-ht	78.8	19
FJI-C1	78.7	20
UPC-21	67	21
JLU-Liu45	42.7	18

Table S5. C_2H_2/CO_2 selectivity performance comparison of some previous reported MOFs.

Compound	Selectivity (0.5:0.5)	Ref.
ZJU-74a	36.5	22
SNNU-65-Cu-Ga	18.7	23
BUT-70A	14.8	24
SNNU-65-Cu-Sc	13.5	23
BUT-70B	11.2	24
ZJUT-2a	10	25
CPM-107	5.7	26
Compound **1**	4.2	This work
UTSA-222	4.0	27
$Cu(BDC\text{-}Br)(H_2O)_{0.5}(DMF)_{2.5}$	3.9	28
ZJNU-100	3.8	29
MFM-127	3.7	30
UPC-112	2.8	31
FJU-36	2.8	32

Table S6. The refined parameters for the DSLF equations fit for the pure isotherms of CO_2, CH_4, C_2H_6, C_3H_8, C_2H_4 and C_2H_2 for compound **1** at 298 K.

	q_{m1}	b_1	n_1	q_{m2}	b_2	n_2	R^2
CO_2	166.64366	0.0025	0.9522	1.00888	6.08931E-4	2.21422	0.99993
CH_4	0.07206	0.1284	1.36881	56.16216	0.00225	1.01347	0.99967
C_2H_6	152.77597	6.91914E-15	5.78602	62.15591	0.05249	0.98972	0.99999
C_3H_8	14.9987	0.06968	0.96147	43.47711	0.80333	1.02696	0.99998
C_2H_4	55.60565	0.03473	0.97379	15.65395	0.00575	0.93268	0.99997
C_2H_2	85.37359	0.00909	0.88842	30.04471	0.05592	0.97088	0.99998

Table S7. The fitting parameters of the virial model with the isotherms at 273 and 298K for CO_2, CH_4, C_2H_6, C_3H_8, C_2H_4 and C_2H_2 for compound **1**.

	a_0	a_1	a_2	a_3	b_0	b_1	b_2	R^2
CO_2	-2605.14006	1.50895	0.24141	-0.01282	11.02857	0.00313	4.7993E-4	0.99999
CH_4	-1815.58629	-148.47707	47.51895	-6.38126	10.39606	0.55578	-0.17381	0.99994
C_2H_6	-3240.78779	-55.26564	2.49881	-0.05038	11.44351	0.19071	-0.00755	0.99998
C_3H_8	-3323.6	-21.07502	0.38401	-0.06539	4.22101	0.47945	-0.00874	0.99985
C_2H_4	-3244.28023	-7.90039	0.8914	-0.02651	11.97116	0.04476	-0.00284	0.99998
C_2H_2	-3291.98574	-14.22141	1.65403	-0.03152	11.99716	0.07767	-0.00625	0.99999

REFERENCES

1. R. Krishna, *Microporous Mesoporous Mater.*, 2014, **185**, 30-50.
2. R. Krishna, *RSC Advances*, 2015, **5**, 52269-52295.
3. R. Krishna, *RSC Advances*, 2017, **7**, 35724-35737.
4. R. Krishna, *Sep. Purif. Technol.*, 2018, **194**, 281-300.
5. R. Krishna, *ACS Omega*, 2020, **5**, 16987-17004.
6. A. L. Myers and J. M. Prausnitz, *A.I.Ch.E.J.* **1965**, *11*, 121-130.
7. Y. Yuan, H. Wu, Y. Xu, D. Lv, S. Tu, Y. Wu, Z. Li and Q. Xia, *Chem. Eng. J.*, 2020, **395**, 125057.
8. D. Geng, X. Han, Y. Bi, Y. Qin, Q. Li, L. Huang, K. Zhou, L. Song and Z. Zheng, *Chem. Sci.*, 2018, **9**, 8535.
9. J. Zhou, T. Ke, F. Steinke, N. Stock, Z. Zhang, Z. Bao, X. He, Q. Ren and Q. Yang, *J. Am. Chem. Soc.*, 2022, **144**, 14322.
10. Y. Zhang, L. Yang, L. Wang, S. Duttwyler and H. Xing, *Angew. Chem. Int. Ed.*, 2019, **58**, 8145.
11. L. Kan, G. Li and Y. Liu, *ACS Appl. Mater. Interfaces*, 2020, **12**, 18642.
12. D. Lin, S. Tu, L. Yu, Y. Yuan, Y. Wu, X. Zhou, Z. Li and Q. Xia, *Ind. Eng. Chem. Res.*, 2023, **62**, 5252.
13. D. Wang, J. Zhang, G. Li, J. Yuan, J. Li, Q. Huo and Y. Liu, *ACS Appl. Mater. Interfaces*, 2018, **10**, 31233.
14. D. Lv, Z. Liu, F. Xu, H. Wu, W. Yuan, J. Yan, H. Xi, X. Chen and Q. Xia, *Sep. Purif. Technol.*, 2021, **266**, 118198.
15. P. Huang, C. Chen, M. Wu, F. Jiang and M. Hong, *Dalton Trans.*, 2019, **48**, 5527.
16. Q. Zhang, X. Lian, R. Krishna, S.-Q. Yang and T.-L. Hu, *Sep. Purif. Technol.*, 2023, **304**, 122312.
17. P. Zhang, X. Wen, L. Wang, Y. Zhong, Y. Su, Y. Zhang, J. Wang, J. Yang, Z. Zeng and S. Deng, *Chem. Eng. J.*, 2020, **381**, 122731.
18. J. Gu, X. Sun, L. Kan, J. Qiao, G. Li and Y. Liu, *ACS Appl. Mater. Interfaces*, 2021, **13**, 41680.

19. J. E. Bachman, M. T. Kapelewski, D. A. Reed, M. I. Gonzalez and J. R. Long, *J. Am. Chem. Soc.*, 2017, **139**, 15363.
20. D. A. Reed, B. K. Keitz, J. Oktawiec, J. A. Mason, T. Runčevski, D. J. Xiao, L. E. Darago, V. Crocellà, S. Bordiga and J. R. Long, *Nature*, 2017, **550**, 96.
21. T. Grancha, M. Mon, J. Ferrando-Soria, J. Gascon, B. Seoane, E. V. Ramos-Fernandez, D. Armentano and E. Pardo, *J. Mater. Chem. A.*, 2017, **5**, 11032.
22. J. Pei, K. Shao, J.-X. Wang, H.-M. Wen, Y. Yang, Y. Cui, R. Krishna, B. Li and G. Qian, *Adv. Mater.*, 2020, **32**, 1908275.
23. J.-W. Zhang, M.-C. Hu, S.-N. Li, Y.-C. Jiang, P. Qu and Q.-G. Zhai, *Chem. Commun.*, 2018, **54**, 2012.
24. Z.-J. Guo, J. Yu, Y.-Z. Zhang, J. Zhang, Y. Chen, Y. Wu, L.-H. Xie and J.-R. Li, *Inorg. Chem.*, 2017, **56**, 2188.
25. H.-M. Wen, C. Liao, L. Li, L. Yang, J. Wang, L. Huang, B. Li, B. Chen and J. Hu, *Chem. Commun.*, 2019, **55**, 11354.
26. H. Yang, T. X. Trieu, X. Zhao, Y. Wang, Y. Wang, P. Feng and X. Bu, *Angew. Chem. Int. Ed.*, 2019, **58**, 11757.
27. J.-x. Ma, J. Guo, H. Wang, B. Li, T. Yang and B. Chen, *Inorg. Chem.*, 2017, **56**, 7145.
28. H. Cui, Y. Ye, H. Arman, Z. Li, A. Alsalme, R.-B. Lin and B. Chen, *Cryst. Growth Des.*, 2019, **19**, 5829.
29. Y. Wang, M. He, X. Gao, X. Wang, G. Xu, Z. Zhang and Y. He, *Inorganic Chemistry Frontiers*, 2019, **6**, 263.
30. J. D. Humby, O. Benson, G. L. Smith, S. P. Argent, I. da Silva, Y. Cheng, S. Rudić, P. Manuel, M. D. Frogley, G. Cinque, L. K. Saunders, I. J. Vitórica-Yrezábal, G. F. S. Whitehead, T. L. Easun, W. Lewis, A. J. Blake, A. J. Ramirez-Cuesta, S. Yang and M. Schröder, *Chemical Science*, 2019, **10**, 1098.
31. W. Fan, X. Wang, X. Liu, B. Xu, X. Zhang, W. Wang, X. Wang, Y. Wang, F. Dai, D. Yuan and D. Sun, *ACS Sustainable Chemistry & Engineering*, 2019, **7**, 2134.
32. L. Liu, Z. Yao, Y. Ye, L. Chen, Q. Lin, Y. Yang, Z. Zhang and S. Xiang, *Inorg. Chem.*, 2018, **57**, 12961.